Electron capture by trapped Ne^{q+} ions at very low energies

M. H. Prior, Richard Marrus, and C. R. Vane*
Department of Physics and Lawrence Berkeley Laboratory, University of California, Berkeley, Berkeley, California 94720
(Received 17 February 1983)

An electrostatic ion trap is used to trap Ne^{q+} ($1 \leq q \leq 10$) ions created by a fast xenon beam passing through neon gas. Decay of a given charge state during the trapping time is due to electron-capture collisions with the ambient gas. Measurement of the decay constant versus density yields a rate constant, from which an effective cross section is derived. Ne^{q+} + Ne ($q=3-10$) and Ne^{q+} + Xe ($q=6-10$) collisions have been studied at mean collision energies in the range 1.0—70.0 eV. Marked oscillation of the effective capture cross sections with charge at fixed mean collision energies is observed. A strong velocity dependence of the effective cross section (rising as the velocity decreases) is observed for several collision pairs.

I. INTRODUCTION

The study of electron capture by low-energy multicharged ions from neutral targets has been motivated mainly by the relevance of this process to fusion devices[1] and astrophysical applications.[2] Moreover, since the capture usually occurs into a state of high principal quantum number, there has been some speculation that ions produced in this way could possibly be used to produce an x-ray laser.

Theoretical modeling of the electron-capture process has mainly been based on the concept of the quasimolecule (A^{q+}-B) which is formed in the reaction $A^{q+}+B \rightarrow A^{(q-1)+}+B^{+}$. The cross sections are determined by the behavior at the avoided crossings of the potential-energy curves of the A^{q+},B initial state and the $A^{(q-1)+},B^{+}$ final state. The predictions of these models for the q dependence of the cross sections are summarized by Olson.[3] In general, the cross sections behave monotonically in q with very little velocity dependence over the range 10^6—10^8 cm/sec because of the availability of the large number of product channels. An interesting exception noted by Olson is the orbiting or Langevin model which should be valid at very low energies. In this model, the cross section is predicted to vary as q/v.

A model which predicts capture cross sections whose dependence on q departs from purely monotonic behavior is that of Ryufuku *et al.*[4] In this model, an electron initially bound to a neutral target atom will transfer to a highly ionized projectile only when certain energy conservation considerations are met. First, the potential-energy function of the electron in the field of projectile and target atoms must allow classical transfer. Second, a resonance condition must obtain in which the binding energy of the electron to the target equals the energy of the level into which the electron will transfer. This model predicts a strong oscillatory dependence of the cross section on q. It further predicts that electron transfer takes place into specific states of high principal quantum number n which can be easily calculated.

On the experimental side, electron capture by low-energy multicharged ions has been a very active area of research since about 1975. Progress is due mainly to, and parallels the development of, multicharged-ion sources, particularly the electron-beam ion source (EBIS), the Penning ionization gauge (PIG) source, and the electron cyclotron resonance (ECR) source. There are several recent reviews of this experimental work.[5] Most of the data obtained with these sources are confined to the energy range >1 keV$\times q$. Recently Phaneuf[6] has utilized a laser source to produce multicharged ions for electron-capture studies with energies as low as about 100 eV. In general, the results tend to support the predictions of the quasimolecule calculations. Several of the experiments, particularly at the lower end of the energy range, show oscillatory behavior of the total cross sections as a function of q (see Refs. 7—12).

One of the newest of the ion sources to be used in the study of electron capture, and the one employed in this work, is the recoil ion source (RIS). The RIS technique is based upon the general observation that a fast, highly ionized projectile from an accelerator when passed through a gas of neutral atoms will produce highly ionized species with high cross section.[13] Although the production process is not fully investigated, experiments at low energy[14] indicate that the cross section for production of a given ion charge state q increases strongly with the charge state of the projectile and decreases slowly with increasing projectile energy. Further, because the production takes place at relatively large distances, the energy transferred to the target is low and can be estimated to be in the range a few eV$\times q$. The RIS technique thus makes available multicharged ions of quite high q at energies that are substantially lower than the sources cited above.

Use of the RIS technique to study the problem of electron capture has been pioneered at Kansas State University (KSU) by Cocke *et al.*[10] and at Gesellschaft für Schwerionenforschung (GSI)—Darmstadt by Beyer, Mann, and collaborators.[15] These studies also give evidence of the cross-section oscillations predicted by the semiclassical model. The KSU results further indicate a very weak velocity dependence or one which decreases slowly with decreasing velocity.

In this paper an experiment is described which also employs the RIS technique. Through the use of an ion trap, total capture cross-section measurements are extended to substantially lower mean kinetic energies (<1 eV$\times q$). As will be seen, the results also show effective cross sections

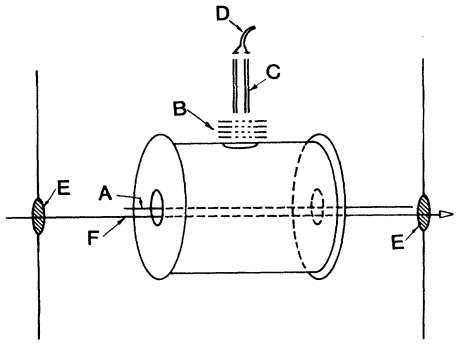

FIG. 1. Electrostatic ion trap. A, central wire; B, acceleration-deceleration grids; C, quadrupole m/q analyzer; D, channel electron multiplier; E, vacuum isolation foils; F, beam axis.

which exhibit strong oscillations as a function of the charge q. They further exhibit the onset of a regime where the cross sections for some of the reactions *increase* with decreasing projectile velocity. Preliminary reports[16] of a portion of this work have previously appeared.

II. EXPERIMENTAL METHOD

Briefly summarized, our technique utilizes an electrostatic ion trap to confine low-energy recoil ions made by impact of a pulsed, fast, heavy-ion beam on a tenuous target gas of neon atoms. The population of a given neon ion charge state is followed in time after the beam pulse and the resulting decay curve yields a loss rate constant. The decay is caused by collisions with the ambient gas in the ion-trap chamber. This gas and its density can be varied and measurements of decay rates versus perturbing gas density yield collision rate constants from which an effective cross section can be inferred. The predominant loss mechanism is electron capture and these measurements provide systematic studies of the charge, velocity, and target dependence in the very low velocity regime (≈ 0.3—3.0 eV/amu). The details of the technique follow.

The recoil neon ions are made by 475-MeV Xe^{27+} beams from the Lawrence Berkeley Laboratory SuperHILAC which enter and exit our ultrahigh-vacuum chamber through carbon foils. We have used foils of 150- and 350-$\mu g/cm^2$ thickness and the mean charge for the foil

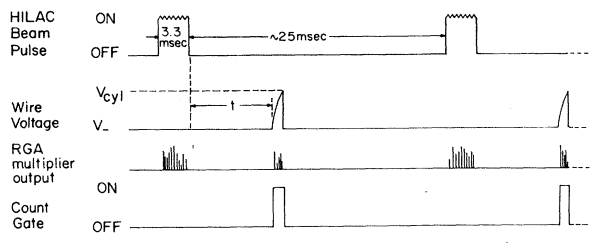

FIG. 2. Timing diagram of the experiment. For collection of ion decay curves t is advanced in synchronism with the multichannel scalar channel number.

transmitted beam (calculated with a formula given by Betz[17]) was Xe^{38+}. It was necessary to use this foil isolation scheme in order to maintain a base vacuum in our chamber a factor of 100 to 1000 lower than the typical few times 10^{-6}-Torr pressure in the accelerator beam line. In the early phases of this work, a number of runs were made with various available heavy-ion linear accelerator (HILAC) beam ions and energies in order to determine which would give the best yield of highly stripped neon recoil ions. Our observations in this regard were qualitatively in agreement with those of Cocke[13] in that the production cross sections grow with the beam ion charge but fall with increasing beam energy. These observations coupled with consideration of available beam currents led us to choose xenon ions at 3.5 MeV/amu as a suitable production beam.

Figure 1 shows a sketch of the electrostatic ion trap and ion detector. All of this is contained in a stainless-steel chamber evacuated by a mechanical cryopump. The ion trap is of the type first described by Kingdon[18] consisting of a conducting cylinder coaxial with a metal wire. In our case the cylinder (15-cm diameter by 18-cm length) and its ends were made from oxygen-free high-conductivity (OFHC) copper and the wire was either 78-μm diameter tungsten or 13-μm diameter gold plated tungsten. The HILAC beam was collimated to about 1.25-cm diameter and passed through the trap parallel to the wire and offset 1.25 cm below it. To allow entrance and exit of the beam, the trap end plates have 5.0-cm diameter holes centered on the wire to preserve rotational symmetry. Small stainless-steel tubes (3.2-mm diameter, not shown in Fig. 1) surround the wire outside the cylinder with their ends adjusted to lie in the plane of the end plates. A trim potential applied to these tubes can largely compensate for the 5.0-cm holes and their small size does not obstruct the beam.

With the wire at a negative potential with respect to the cylinder, recoil ions orbit about the wire and are confined longitudinally by the potential well created by the end plates and tubes. The stored ions are analyzed by raising the wire potential to that of the cylinder and sampling that portion which escape radially through a grid covered hole. This dumped ion sample passes through a series of grids and into a commercial (EAI QUAD 250) radio-frequency (rf) quadrupole residual-gas analyzer (RGA). This device contains a channel electron multiplier (CEM) normally used as a current amplifier for detection of ions made by the electron-impact ionizer supplied with the instrument. In this work, because of the pulsed nature of our "source" and the small number of detected ions, we count ion pulses from the CEM anode using standard pulse counting techniques. Some care was needed in doing so as to filter out a radio-frequency signal arising from the rf voltage applied to the quadrupole rods.

A timing diagram of the operation of the ion-trap-RGA combination is shown in Fig. 2. The HILAC is a pulsed machine with a typical beam pulse lasting 3.3 msec and a 36-Hz repetition rate. Thus ions created and captured during the beam pulse can be held by the trap for any desired portion of the approximately 25 msec between pulses. This is indicated in the second line of Fig. 2, where the rise of the wire potential is shown occurring at a time t after the beam pulse. Because the CEM in the RGA has a direct view of the HILAC beam, a number of

pulses are always observed during the beam pulse even though the trap is not set to dump positive ions. These are caused by prompt photons and perhaps high-energy electrons created in the beam-gas collision. A count gate synchronous with the trap dump pulse ensured that we registered only counts occurring during the dump period. Normally a slow rise time (≈ 0.5 msec) is used when dumping the trap in order to avoid pulse pileup in the CEM signal channel (this was important only for the more populous charge states). This spreads out the ion arrival times at the CEM cathode. However, for time-of-flight studies of the velocity distribution of the trapped ions, a fast rising (less than 1.0 μsec) dump pulse was used and pulse pileup (if present) was avoided by limiting the number of trapped ions. This procedure avoids perturbing the velocity distribution that exists just prior to the dump pulse.

The ion trap was operated in one of three modes which we label m/q, decay, and TOF (time of flight). In the m/q mode, the delay t is held fixed and the RGA program voltage is stepped in synchronism with the channel advance of the computer controlled multichannel scalar receiving the CEM counts. In this way the RGA can be swept over a selected range of mass to charge ratio (m/q) values to determine the charge distribution of the trapped neon ions (together with any trapped ions made from the background gas).

In the decay mode, the RGA is set to monitor a particular charge-state neon ion and the delay time t is stepped in sync with the multichannel scalar. This produces curves showing the decay of the selected charge state during the period between HILAC pulses. In both m/q and decay modes the dwell time in any channel is that required to integrate the HILAC beam current to a preset charge value. This compensates for beam current variation during the data collection period. The current integration is performed by an integrating electrometer connected to a Faraday cup at the end of the beam line.

Finally, in the TOF mode with the RGA set to monitor one charge state and t fixed, the computer is used in a pulse height analysis mode to accumulate CEM pulses processed by a time-to-height converter started on the rise of the wire dump pulse. This produces a time-of-flight distribution for the chosen charge state.

The motion of ions in the electrostatic trap is a complicated problem in classical dynamics since the general potential[19] is not a simple function. However, in our case the geometry is such that we detect only those ions which move in orbits close to the trap midplane where the potential $\Phi(r)$ at radius r is accurately approximated as that of an infinite coaxial system

$$\Phi(r) = V \frac{\ln(r/R)}{\ln(R/w)} , \tag{2.1}$$

where V is the potential difference between the cylinder and the wire, and R and w are the cylinder and wire radii, respectively. Ion orbits in this potential have been calculated by Hooverman.[20] They have the interesting and useful property that, regardless of initial conditions, the mean kinetic energy is the same for all orbits, a property unique to the logarithmic potential. This is a consequence of the virial theorem which predicts

$$\langle T \rangle = \frac{qeV}{2\ln(R/w)} , \tag{2.2}$$

where T is the kinetic energy of an ion with charge qe and the brackets indicate a time average. This property of the logarithmic potential was recognized by Talrose and Karachevtsev[21] in ion-molecule reaction studies using a reaction chamber similar to our trap. Thus the root-mean-square (rms) velocity $v_{\rm rms}$ for all orbits of an ion with a given q/m depends only upon the geometry of the trap (R/w) and the trap potential V

$$v_{\rm rms} = \left[\frac{qeV}{m \ln(R/w)} \right]^{1/2} . \tag{2.3}$$

The initial conditions of the ion motion do come into consideration in a real device since, clearly, ions created with arbitrarily large or small initial velocities v_c will collide with the cylinder or wire, respectively. However, the virial theorem result applies to all orbits; hence those ions that are trapped have $v_{\rm rms}$ as given above. This may be only a small comfort, however, if the number of such ions is vanishingly small. The number captured will depend upon the fraction of ions with initial conditions providing orbits within the wire to cylinder space.

The extrema of the radial coordinate r of any orbit are given by the solutions of the equation

$$y^2(x^2 - 2\ln y) = x^2 \sin^2\vartheta_c , \tag{2.4}$$

where $y = r/r_c$ and r_c is the initial value of r, and $x = v_c/v_{\rm rms}$ and ϑ_c is the acute angle made by the initial velocity v_c with respect to the initial radial vector. Setting $r = R$ or w one obtains two angles $\alpha_R(x)$ and $\alpha_w(x)$ which satisfy Eq. (2.4) when substituted for ϑ_c. For all launch angles less than $\alpha_w(x), \alpha_R(x)$ an ion with initial velocity $v_c = x v_{\rm rms}$ will strike the wire or cylinder, respectively. Thus, confined ions are restricted to angles ϑ_c greater than the larger of α_w, α_R; when this reaches $\pi/2$ no ions will be trapped.

One can easily determine that $\alpha_R(x)$ is a very strong function of x, switching from a very small value to $\pi/2$ over a small range. For our case, where r_c ranges from 0.78 to 1.78 cm (corresponding to the position and extent of the HILAC beam), this switching occurs at $x \approx 1.9$; for x less than 1.72 all orbits clear the cylinder; for x greater than 2.14, all orbits do not. Thus we cannot confine ions in a potential such that $\langle T \rangle$ is less than about $\frac{1}{4}$ of the recoil energy. In fact, we observed, for example, that the number of trapped Ne^{10+} ions fell strongly as the trap potential was reduced to ≈ 5 V. This corresponds to $\langle T \rangle \approx 3$ eV indicating a recoil energy of about 12 eV.

An upper limit on $\langle T \rangle$ is placed by $\alpha_w(x)$ which has a less strong behavior. For the larger wire used ($w = 38$ μm) no ions would be trapped with x less than 0.0075 with the fraction confined falling to 50% at about $x = 0.015$, which, for a recoil energy of 10 eV, would correspond to $\langle T \rangle = 44$ KeV. The requirement for pulsed kilovolt potentials, plus the decreased resolution of the RGA for fast ions (due to the short transit time) inhibit use of the trap-RGA combination described here near this upper limit.

In order to extract rate constants from our decay measurements, it was necessary to measure absolute changes in the perturbing gas density in the range $1-10\times10^{10}$ cm^{-3}

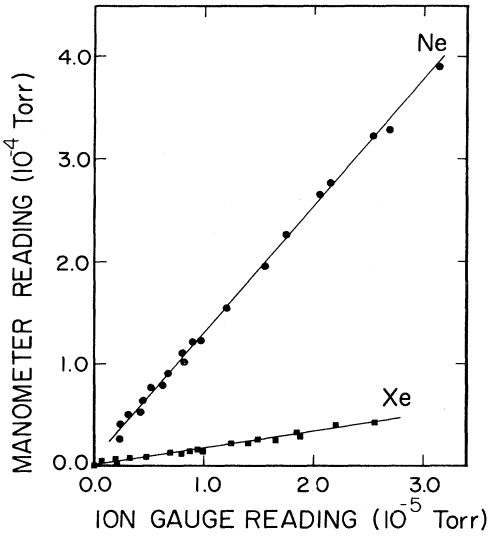

FIG. 3. Example of calibration data for determination of absolute pressure increments with the nude ion guage.

($3-30\times10^{-7}$ Torr). This was done using a nude Bayard-Alpert ionization gauge which was calibrated before and after each accelerator run against a capacitance manometer. The comparison was accomplished at higher pressures where the two instruments have overlapping ranges. To limit space-charge effects, the ion gauge was operated with reduced emission current (1 mA instead of the normal 4 mA). An example of calibration data for neon and xenon is shown in Fig. 3. All that is required for this work is the slope of these lines and we rely on the linearity of the ion gauge to determine pressure changes absolutely in the 10^{-7}- to 10^{-6}-Torr range where measurements were made. We estimate our target density calibration error to be $\pm15\%$.

A dual gas handling system controls admission of neon and xenon gases into the trap chamber through separate motor operated variable leak valves. Thus, the density of either gas can be independently controlled. The gas handlers are constructed primarily of glass with approximately 1.5-liter ballast volumes for gas storage. During data collection the total gas pressure in the trap chamber was monitored continuously with the nude ionization gauge.

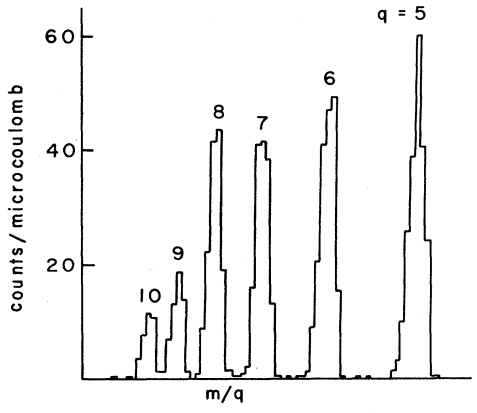

FIG. 4. An m/q scan of trapped $^{22}Ne^{q+}$ ions ($q\geq5$). Delay time (see Fig. 2) was less than 0.5 msec. Vertical scale is normalized to the Xe ion beam charge accumulated in the downstream Faraday cup.

III. DATA PRESENTATION AND ANALYSIS

Initially, experiments were carried out to determine the beam conditions (energy and ion) which would give the largest yield of the highest neon charge states. These experiments were performed with the ion-trap timing set for the m/q mode (see Sec. II). In this way, a series of peaks were observed which correspond to the distribution of the various charge states of neon present in the ion trap at an arbitrary time interval after the HILAC pulse had passed. A sample of such a charge-state distribution is shown in Fig. 4. The lowest charge states (Ne^{q+}, $q\leq4$) were not included in the scan. The signal-to-noise ratio during any given run was determined largely by the ambient background gas pressure and composition. Particularly troublesome was water vapor, since the H_2^+ fragment has an m/q value virtually identical to that of $^{20}Ne^{10+}$. To avoid this problem the neon used in all runs was enriched to 99.9% ^{22}Ne; the RGA detection system easily resolves $^{22}Ne^{10+}$ from H_2^+.

It is worth pointing out that the integrated area under the m/q peaks, Fig. 4, cannot be taken directly as a measure of the production cross section for a particular charge state. It cannot be assumed that the transmission of the RGA is the same for all charges. In fact, the operating parameters were generally adjusted so as to optimize resolution of the highest charge ions; this had the effect of reducing the transmission of the more abundant lower charge states. Also, the time evolution of the population of a particular charge state depends upon several production and loss mechanisms. This can be summarized by the rate equation:

$$\frac{dN_q}{dt}=I\Delta z\sigma_q n_0 + n_0\sum_{q'>q}N_{q'}\langle v_{q'}\sigma_{q'q}\rangle - n_0N_q\sum_{q'<q}\langle v_q\sigma_{qq'}\rangle\ , \tag{3.1}$$

where σ_q is the production cross section for charge q, I is the HILAC beam particle current, Δz is the effective length of the trap, n_0 is the density of neon atoms, N_q is the number of trapped neon ions of charge q, and $\sigma_{q'q}$ is the electron-capture cross section for charge q' impacting upon a neon atom with relative velocity $v_{q'}$ to produce a charge q. This equation describes the secular variation of N_q and is valid providing the ion orbit frequencies ($\approx10^5$ Hz) are much higher than the rate of variation of N_q ($\approx10^3$ Hz). A further approximation in writing Eq. (3.1) is that the time averages, e.g., $\langle v_q\sigma_{qq'}\rangle$, are not strongly dependent upon the initial velocity and launch angle (v_c,ϑ_c) of the charge q ion. The first term in Eq. (3.1) described production of charge q ions by the heavy-ion beam, the second describes feeding of the population of

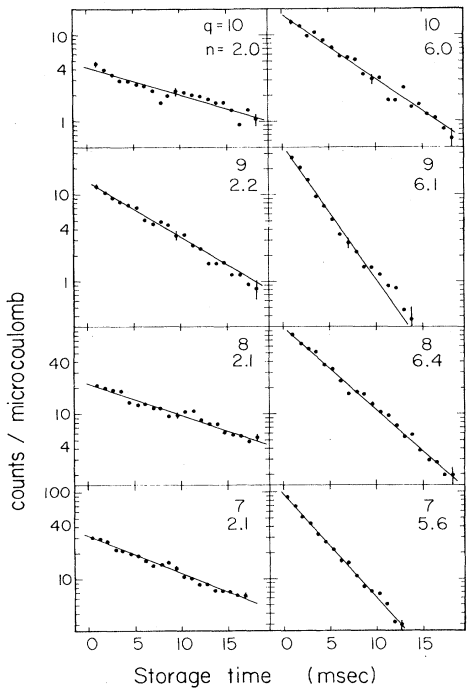

FIG. 5. Examples of decay curves for Ne^{q+} ions ($q=7-10$) in Ne at two densities n (in units of 10^{10} cm^{-3}). Trap potential was adjusted to maintain $v_{rms}=9.6\times10^5$ cm/sec for each ion.

charge q by higher charges via electron-capture collisions, and the third accounts for loss of charge q by electron-capture resulting in lower charge states, As will be discussed below, our detection system is sensitive primarily to those ions produced by the HILAC beam. Thus, we neglect the second term in Eq. (3.1). Further, we define

$$s_q=\sum_{q'<q}\sigma_{qq'},$$

and then one has

$$\frac{dN_q}{dt}=I\Delta z\sigma_q n_0-\langle s_q v_q\rangle n_0 N_q . \tag{3.2}$$

The solution for N_q at a time t after the HILAC pulse of duration t_H is

$$N_q=I\Delta z\sigma_q n_0(1-e^{-\gamma_q t_H})e^{-\gamma_q t},$$

where $\gamma_q=\langle s_q v_q\rangle n_0$. Thus, only in the limit of small $\gamma_q t_H,\gamma_q t$ will the m/q peaks be proportional to the production cross section σ_q with a proportionality constant independent of q. At increased densities n_0 such that $\gamma_q t_H$ becomes large, the yield saturates. If the capture cross sections vary substantially between charges it is then possible to have some yields saturated while others are not. Generally, however, our observations are consistent with production cross sections which increase monotonically as q decreases.

Observation of the decay of a particular charge held in the ion trap between beam pulses can give information about the velocity averaged electron-capture cross sections. Figure 5 shows a set of decay curves for Ne^{q+} ions ($q=7-10$) at two neon gas densities. The trap potential was adjusted so that the mean kinetic energy of the ions was the same, 10.6 eV, for all the charge states. To a good approximation, these curves are well fit by single exponentials of the form

$$N_q=N_q(0)e^{-\Gamma_q t}, \tag{3.3}$$

where Γ_q is a decay constant and $N_q(0)$ is the signal size at $t=0$ (usually measured from the end of the HILAC beam pulse). There are a number of effects which one might expect to give rise to a more complicated nonexponential behavior in the time evolution of the trapped ion population. First, for all charge states less than fully stripped (Ne^{10+}), the population of charge q can be enhanced in time by ions with charge $q'>q$ which undergo single or multiple electron capture. This is the second term in Eq. (3.1) neglected in the discussion above. Inclusion of this cascade feeding process could give rise to nonexponential behavior. We do not observe these effects because of two factors. First, the lower charge states are generally produced with higher yields, thus one is faced with observing the effects of feeding from a smaller population onto a larger directly produced population. More importantly, however, there is a discrimination in the ion detection scheme in favor of ions produced by the HILAC beam. This arises because the distribution of orbits of HILAC-produced ions is strongly perturbed by the Coulomb "explosion" which occurs between the two ions following an electron-capture collision. The energy available to the two products of an electron-capture collision, with a single electron transferred, is approximately

$$E_x=\frac{(q-1)e^2}{R_x}, \tag{3.4}$$

where R_x is the internuclear separation at which the transfer occurs. In terms of the one-electron-capture cross section, R_x may be estimated to be

$$R_x\approx\left[\frac{2}{\pi}\sigma_{q,q-1}\right]^{1/2}. \tag{3.5}$$

E_x can be a large fraction of, or even exceed, the mean kinetic energies of the ions studied in this work. Of course, the fraction of E_x transferred to the neon ion of charge $q-1$ depends upon the mass of the companion singly charged product. In the case of $Ne^{q+}+Ne$ collisons, 50% is transferred to the $Ne^{(q-1)+}$ ion, whereas in collision with Xe the share is 86%.

As an example, consider $Ne^{9+}+Ne$. Here our observations indicate an effective cross section for capture of about 5×10^{-15} cm^2 at a mean kinetic energy of 10.5 eV [from the virial theorem Eq. (2.2)]. One calculates $E_x\approx23$ eV, of which half goes to the product Ne^{8+} ion. The mean kinetic energy of Ne^{8+} ions in the same trap potential (22.0 V) is 9.3 eV. This large injection of energy causes the Ne^{8+} products to occupy greatly expanded orbits as compared to the Ne^{8+} produced by the HILAC beam. In fact, a large fraction of the product ions will collide with the trap cylinder or ends and be lost.

This behavior has been studied in detail using a numerical model, which determines the orbit distribution following collisions and calculates the resultant signal intensity

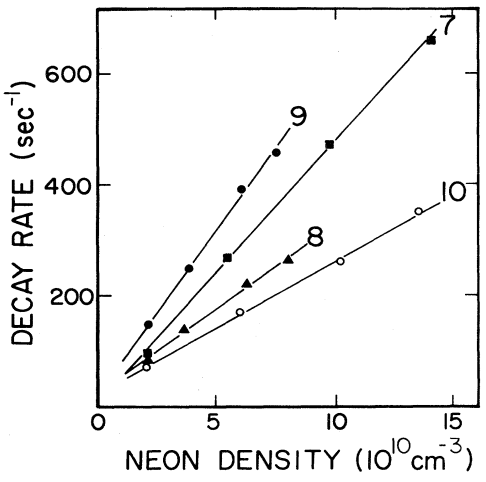

FIG. 6. Variation of the decay rates for Ne^{q+} ($q=7-10$) ions vs Ne density. Slopes of these curves are $\langle vs_q \rangle$.

for the geometric arrangement of the ion trap and ion detector used here. The model assumes that the ion trap can be represented as a superposition of a logarithmic radial potential and a one-dimensional harmonic-oscillator potential along the z (wire) direction. Calculations of the exact potential distribution (see, e.g., Ref. 19) show that this is a reasonable approximation. Ions are created by the heavy-ion beam uniformly along its length parallel to the z axis. The initial velocity distribution along the z axis is assumed to be thermal at the temperature of the target (neon) gas. This would be the case for recoil of the Ne^{q+} ions at exactly 90° to the HILAC beam.

The calculations assume strong collisions between the recoil ions and neutral target atoms; i.e., collisions in which the products are scattered isotropically in the center of mass. This is not appropriate at higher energies but becomes so as one enters the orbiting regime appropriate to the low-energy ion-atom collisions studied here. Elaboration of the results of these calculations will not be presented here. However, in terms of the $Ne^{9+}+Ne$ example discussed above, they show that the detection efficiency for the product Ne^{8+} ions would be only about 20% of that for the Ne^{+8} ions made by the HILAC beam. In collision with xenon, the reduction remains about 20% because, although the fraction of E_x transferred to the Ne^{8+} ion is larger, E_x itself is reduced by about a factor of 2 due to the approximately fourfold increase in the capture cross section in this case.

Another possibility for obtaining nonexponential behavior arises if the capture cross section is highly velocity dependent, and if there is a wide distribution of orbits (and hence velocities) in the trap. Then the capture rate will vary strongly with the orbit parameters. Within the uncertainties of this experiment, however, no such effects have been observed in $Ne^{q+}+Ne$, Xe collisions. Thus, the decay curves are fit to a single exponential (plus constant background in some cases) and the decay constant Γ_q extracted.

Γ_q is related to the electron-capture cross section by

$$\Gamma_q = \langle vs_q \rangle n + \Gamma_0 , \tag{3.6}$$

where n is the target gas density (Ne or Xe), and Γ_0 is the loss rate associated with all mechanisms not proportional to the gas density n. These include escape of ions from the trap field and electron capture from background gases present. (There is always neon gas present; so when studying capture from xenon the capture rate on neon appears in this term.)

From Eq. (3.6) one sees that the rate constant $\langle vs_q \rangle$ may be obtained by measuring the decay constant Γ_q at several values of the gas density n. The slope of the resultant straight line is $\langle vs_q \rangle$. This requires collection of a series of decay curves such as shown in Fig. 5; usually at least four different densities are used for each charge and trap potential. Plots of Γ_q vs n are shown in Figs. 6 and 7. It is seen that the expected linear relationship is obtained. This technique has been used to measure rate constants for $Ne^{q+}+Ne$ ($3 \le q \le 10$) and $Ne^{q+}+Xe$ ($6 \le q \le 10$), for a range of trap potentials.

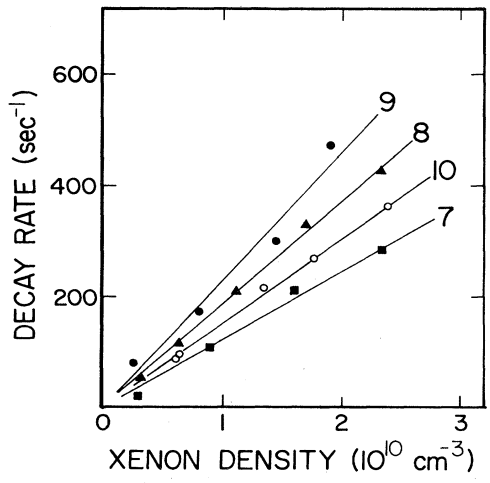

FIG. 7. Variation of the decay rates for Ne^{q+} ($q=7-10$) ions vs Xe density. Slopes of these curves are $\langle vs_q \rangle$. Note the scale change of the density axis in comparison to Fig. 6. Curves have been displaced vertically to have a common intercept at the origin.

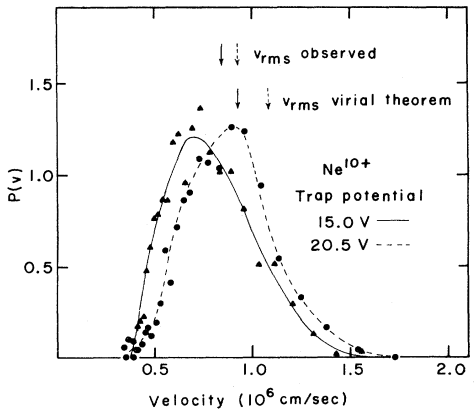

FIG. 8. Example of TOF data for Ne^{10+} ions at two trap potentials. The lines are to guide the eye. Observed v_{rms} values are calculated from the data.

The measured rate constants $\langle vs_q \rangle$ can be converted to effective cross sections by division with an appropriate velocity. To this end we note that each ion exhibits, in general, a distribution of velocities as it orbits the wire and oscillates along the trap axis (z direction). The geometry of our detection system is such that the ions which orbit near the midplane of the trap are preferentially detected over those with large z-motion amplitudes. In fact, the sensitivity to ions with amplitude A falls as A^{-1}. Thus, the velocity distribution of the ions detected is well approximated as that appropriate for ions orbiting in a pure logarithmic potential, and we use the rms velocity calculated from Eq. (2.3) to convert rate constants into effective cross sections. Thus,

$$\sigma_{\text{eff}}(v_{\text{rms}}) = \frac{\langle vs_q \rangle}{v_{\text{rms}}} .$$

Neglect of the z motion amounts to an error in v_{rms} of less than $\approx 5\%$. $\sigma_{\text{eff}}(v_{\text{rms}})$ is thus a velocity averaged cross section with a relationship to the true cross section $s_q(v_{\text{rms}})$ which depends upon the form of the velocity dependence of s_q and the distribution of ion velocities. One obtains $\sigma_{\text{eff}} = s_q$ for two special cases; namely, when $s_q(v)$ is proportional to v or v^{-1}.

To test the assumption that v_{rms} as deduced from the Virial Theorem Eq. (2.3) is a good representation of the true value for the detected ions, the trap was operated in the time-of-flight mode (see Sec. II) and the distribution of arrival times for ions exiting from the trap was recorded. The arrival time distributions were converted to velocity distributions by assuming that all ions originate from the position of the central wire. This approximation is reasonable since the ions are created at about 1.3 cm from the wire and, under most trap conditions, their low recoil energy will result in orbits which do note extend much beyond this radius. The total distance from the wire to the channel electron multiplier in the RGA is 35 cm. Samples of velocity distributions derived for Ne^{10+} ions in two trap potentials are shown in Fig. 8. One sees that the distribution for the higher potential (20.5 V) is shifted to higher velocity and that there is reasonable agreement between the virial theorem value for v_{rms} and that calculated from the distributions in the figure.

TABLE I. Effective cross section (10^{-15} cm^2) vs v_{rms} for Ne^{q+} + Ne collisions. Bottom row contains the CB model cross sections.

v_{rms} (10^5 cm/sec)	$q=3$	$q=4$	$q=5$	$q=6$	$q=7$	$q=8$	$q=9$	$q=10$
3.1			10.0					
3.3				9.9				
3.6					9.2			
4.8			7.3	10.1	8.3	3.6	7.6	
5.9	0.90			6.3				
6.3					5.6			
6.8					7.2	3.2		2.8
								2.7
6.9				8.6				
7.5						3.0	6.0	
						2.9		
7.6		3.0	3.8		4.8			3.6
8.3				5.0				
9.5				6.0				
9.6					5.4	3.5	6.1	2.3
9.7								2.5
10.7		2.6	3.1			2.4	4.5	3.0
10.8					4.1			
11.0	0.54							
14.2			2.6		3.4			
15.5						2.2		
16.8							3.2	
16.9		2.4	2.7					2.4
17.1					2.7			
18.5				4.5				
19.0	0.60							
21.0					2.5			
21.6					3.3			
22.4					2.2			
23.6								3.0
23.9							3.6	
24.0		2.1	2.4		2.9	2.2		
25.8				4.0				
CB model		0.27	2.0	0.76	0.43	1.5	0.93	2.5

IV. RESULTS AND DISCUSSION

The results of our measurements are presented in Tables I and II and Figs. 9 and 10. The tables contain the effective cross section σ_{eff} vs v_{rms} for $Ne^{q+}+Ne$ and Xe, respectively, and Fig. 9 contains these data in graphical form. In Fig. 10 we display the variation of σ_{eff} with the Ne ion charge at three values of v_{rms}. Because data were not always collected across the range of q at a common value of v_{rms} we have done some interpolation in order to compose Fig. 10. For clarity, error bars are not present in the figures; but for purposes of relative comparisons the statistical error on the points is estimated to be approximately 10—15% (one standard deviation) for $q \leq 9$ and 20% for $q=10$. The absolute error on the values of σ_{eff} is estimated to be 30%. Our results for Ne^{8+} are in agreement with those obtained by Beyer, Mann, and Folkmann[22] for capture by $(1s2p)^3P_1$ Ne^{8+} at a recoil velocity of about 8×10^5 cm/sec. They obtained cross sections of $3.6\pm1.1\times10^{-15}$ cm^2 and $28.7\pm8.8\times10^{-15}$ cm^2 for Ne and Xe targets, respectively. Since our Ne^{8+} ions are in the $1s^2$ ground state (excited states[23] have decayed before we sample the trap population), the agreement between our σ_{eff} values and those of Beyer *et al.*[22] indicates little dependence upon the inital excitation state of the ion, at least for this case.

One notes that there is a prominent nonmonotonic behavior of σ_{eff} as q changes (Fig. 10). In the more complete $Ne^{q+}+Ne$ data, one also observes an apparent damping of the oscillation as v_{rms} increases. This is consistent with observations of other workers (e.g., Refs. 7—12) at higher energies where oscillations of smaller amplitude are seen. This occurs because the velocity dependence of σ_{eff} varies with q. There is little velocity dependence for $q=8$ and 10 in the $Ne^{q+}+Ne$ results, but strong dependence for $q=5$, 6, 7, and 9. In the data for Xe one is struck by the reversal of "phase" of the oscillation of σ_{eff} at $q=7$ as v_{rms} changes from 5.0 to 10.0×10^5 cm/sec. This is seen in Fig. 9 as the continued rise of σ_{eff} $(q=7)$ at low values of v_{rms} as compared to the other ions in collision with Xe.

TABLE II. Effective cross section (10^{-15} cm^2) vs v_{rms} for $Ne^{q+}+Xe$ collisions. Bottom row contains the CB model cross sections.

v_{rms} (10^5 cm/sec)	$q=6$	$q=7$	$q=8$	$q=9$	$q=10$
3.6	18.9	26.7			
		27.4			
4.8			17.0	21.2	
5.5			16.3		
5.7		20.3			
6.3				25.2	
6.5	18.1	17.2	19.2		16.8
			23.2		
8.2			19.4		
9.6	16.7	13.7	19.2	23.9	15.8
		12.7	17.4	20.9	16.6
			17.5		17.9
14.0	13.7	9.6	16.0	18.4	16.2
15.6		10.0			
17.1		10.3	14.0	18.0	
24.0		9.0	15.1		
24.2	9.6				
CB model	2.4	5.6	3.1	6.1	10.8

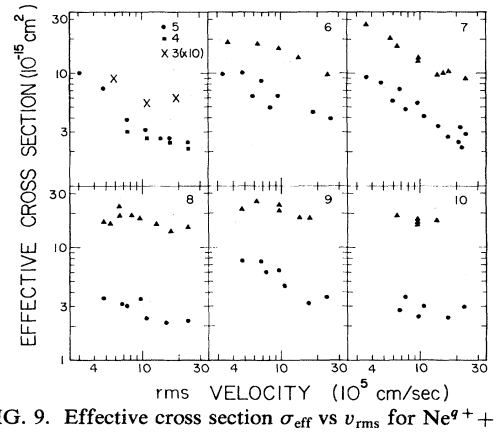

FIG. 9. Effective cross section σ_{eff} vs v_{rms} for $Ne^{q+}+Xe$ (triangles) and $Ne^{q+}+Ne$ (all other points) for $6\leq q\leq10$ Xe) and $3\leq q\leq10$ (Ne). Statistical uncertainty is ±10—15%, for $q\leq10$ and ±20% for $q=10$. Absolute uncertainty is ±30%.

In discussing our results we do so in terms of models and calculations for single electron capture. One must keep in mind, however, that σ_{eff} includes all multiplicities of electron transfer. Cocke *et al.*[24] have shown in studies of $Ar^{q+}+$noble gas collisions that single electron capture predominates for the lighter atoms (e.g., Ne) but that so-called transfer ionization, involving the transient capture of two electrons is comparable to ordinary single capture in collisions with Xe. Such a process if present at the lower velocities in this work (about a factor of 10 below those in Ref. 24) would be included in our σ_{eff}.

Oscillation of the single-electron-capture cross section as the charge of the projectile is varied has been observed by other researchers (see Refs. 7—12) at impact velocities exceeding $\approx10^7$ cm/sec. The often invoked theoretical model with which the results of these studies are com-

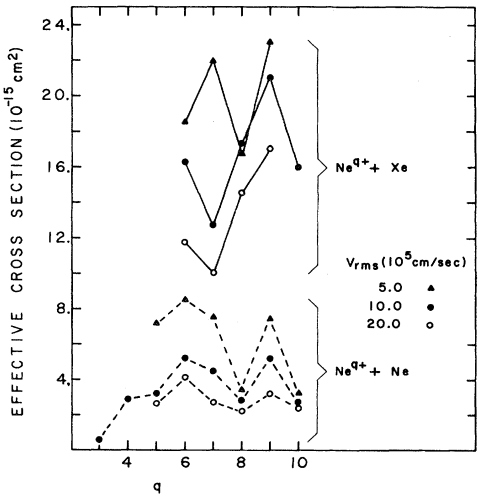

FIG. 10. Effective cross section σ_{eff} vs q at three values of v_{rms}. The points have been interpolated from the data (Tables I and II and Fig. 9). Relative uncertainty in the points is approximately ±15%.

pared is the classical over barrier model (CB) introduced by Ryufuku *et al.*[4] This mode is generally successful in predicting the principal quantum number of the Rydberg level occupied by the active electron in the $q-1$ charged product ion. This has been verified by x ray and Auger-electron spectroscopy following capture at impact energies of a few eV by Beyer, Mann, and co-workers (for a review of this work and further references see Ref. 25). It has also been verified by kinetic energy analysis of the forward scattered $(q-1)+$ ions at collision energies of a few hundred eV.[26,27] The CB model contains no velocity dependence; it was formulated for comparison with measurments made at higher impact energies than studied here, where only weak velocity dependence has been observed (for $q \geq 5$). We have included cross sections calculated with the CB model in Tables I and II. One sees that the magnitudes, perhaps not surprisingly, are in poor agreement with σ_{eff} in most cases. Of more importance, however, is the lack of agreement with the phase of the oscillations with q. This lack of phase agreement has been noted[12,27] in measurements made at higher energies as well.

The simplest model predicting a velocity dependence for the single-electron-capture cross section is the orbiting model first proposed by Gioumousis and Stevenson[28] to explain ion-molecule reaction studies. Here the long-range R^{-4} polarization potential leads to a cross section proportional to q/v. The v^{-1} dependence is not far from that observed here for those collision pairs showing the strongest variations with velocity (e.g., $q=5$, 6, 7, and 9 on Ne and $q=7$ on Xe). Of course, a more complete quantal calculation will be required in order to expect to obtain the proper charge and velocity dependence for the capture cross sections pertinent to this work. In this regard, we note that recently Bottcher and Heil[29] have carried out such calculations for collisions of Be^{4+}, B^{5+}, and $C^{4,5,6+}$ with H. The agreement with existing data of Phaneuf[6] for the carbon ions in the energy range $\approx 15-300$ eV is encouraging. It is also interesting to note that a Landau-Zener treatment, including curved trajectories, shows remarkable agreement with the velocity dependence of the single-electron-capture cross section calculation by more elaborate quantal methods in the cases C^{3+} and N^{3+} on H.[30–32] It is hoped that continuing theoretical efforts will successfully address the multicharged ion-atom systems containing considerably more electrons (such as those studied here) in the low-velocity ($\leq 10^7$ cm/sec) regime.

ACKNOWLEDGMENTS

We wish to extend thanks to Charles Munger for help in collecting some of the data presented here, and make note of the valuable assistance provided by Dr. Harvey Gould, Mr. Douglas MacDonald, and the operators and staff of the Lawrence Berkeley Laboratory SuperHILAC. This work was supported by the Director, Office of Energy Research, Office of Basic Energy Sciences, Chemical Sciences Division of the U.S. Department of Energy under Contract No. DE-AC03-76SF00098.

*Present address: Oak Ridge National Laboratory, P.O. Box X, Oak Ridge, TN 37830.

[1]H. B. Gilbody, in *Advances in Atomic and Molecular Physics,* edited by D. R. Bates and B. Bederson (Academic, New York, 1979), Vol. 15, p. 293.

[2]A. Dalgarno, Ref. 1, p. 37.

[3]For a summary and many relevant references therein, see R. E. Olson, in *Electronic and Atomic Collisions,* edited by N. Oda and K. Takayanagi (North-Holland, Amsterdam, 1980), p. 391.

[4]H. Ryufuku, K. Sasaki, and T. Watanabe, Phys. Rev. A 21, 745 (1980).

[5]E. Salzborn and A. Muller, Ref. 3, p. 407; F. J. Detteri, in *Atomic and Molecular Processes in Controlled Thermo-nuclear Fusion,* edited by M. R. C. McDowell and A. M. Ferendeci (Plenum, New York and London, 1980), p. 351.

[6]R. A. Phaneuf, Phys. Rev. A 24, 1138 (1981); R. A. Phaneuf, I. Alvarez, F. W. Meyer, and D. H. Crandall, *ibid.* 26, 1892 (1982).

[7]D. H. Crandall, R. A. Phaneuf, and F. W. Meyer, Phys. Rev. A 19, 504 (1979); 22, 379 (1980).

[8]S. Bliman, J. Aubert, R. Gellin, B. Jacquot, and D. Van Houtte, Phys. Rev. A 23, 1703 (1981).

[9]S. Bliman, S. Dousson, B. Jacquot, and D. Van Houtte, J. Phys. (Paris) 42, 1387 (1981).

[10]C. L. Cocke, R. Dubois, T. J. Gray, and E. Justiniano, IEEE Trans. Nucl. Sci. 28, 1032 (1981); E. Justiniano, C. L. Cocke, T. J. Gray, R. D. DuBois, and D. Can, Phys. Rev. A 24, 2953 (1981).

[11]H. Schrey and B. A. Huber, J. Phys. B 14, 3197 (1981).

[12]T. Iwai, Y. Kaneko, M. Kimura, N. Kobayashi, S. Ohtani, K. Okuno, S. Takagi, H. Tawara, and S. Tsurubuchi, Phys. Rev. A 26, 105 (1982).

[13]I. A. Sellin *et al.*, Z. Phys. 283, 320 (1977); C. L. Cocke, Phys. Rev. A 20, 749 (1979).

[14]T. J. Gray, C. L. Cocke, and E. Justiniano, Phys. Rev. A 22, 849 (1980).

[15]R. Mann, F. Folkmann, and H. F. Beyer, J. Phys. B 14, 1161 (1981).

[16]C. R. Vane, M. H. Prior, and R. Marrus, Phys. Rev. Lett. 46, 107 (1981); R. Marrus, M. Prior, and C. R. Vane, Nucl. Instrum. Methods 202, 171 (1982).

[17]H.-D. Betz, Rev. Mod. Phys. 44, 465 (1972).

[18]K. H. Kingdon, Phys. Rev. 21, 408 (1923).

[19]M. H. Prior and E. C. Wang, in *Atomic Physics 5,* edited by R. Marrus, M. Prior, and H. Shugart (Plenum, New York 1977), p. 125.

[20]R. H. Hooverman, J. Appl. Phys. 34, 3505 (1963).

[21]V. L. Talrose and G. V. Karachevtsev, in *Advances in Mass Spectrometry,* edited by W. L. Mead (Elsevier, Amsterdam, 1966), Vol. 3, p. 211.

[22]H. F. Beyer, R. Mann, and F. Folkmann, J. Phys. B 15, 1083 (1982).

[23]The "metastable" $1s2s\ ^1S_0$ and $^3S_1$ states have lifetimes of 0.1 and 91 μsec, respectively. See, for example, the calculations of C. D. Lin, W. R. Johnson, and A. Dalgarno, Phys. Rev. A 15, 154 (1977).

[24]C. L. Cocke, R. Dubois, T. J. Gray, E. Justiniano, and C. Can, Phys. Rev. Lett. 46, 1671 (1981).

[25]R. Mann and H. F. Beyer, Comments At. Mol. Phys. 12, 149 (1982).

[26]S. Ohtani, Y. Kaneko, M. Kimura, N. Kobayashi, T. Iwai, A.

Matsumoto, K. Okuno, S. Takagi, H. Tawara, and S. Tsurubuchi, J. Phys. B 15, L535 (1982).
[27]R. Mann, C. L. Cocke, A. S. Schlacter, M. Prior, and R. Marrus, Phys. Rev. Lett. 49, 1329 (1982).
[28]G. Gioumousis and D. P. Stevenson, J. Chem. Phys. 29, 294 (1958).
[29]C. Bottcher and T. G. Heil, Chem. Phys. Lett. 86, 506 (1982).
[30]W. D. Watson and R. B. Christensen, Astrophys. J. 231, 627 (1979).
[31]R. McCarroll and P. Valiron, in *Electronic and Atomic Collisions,* edited by N. Oda and K. Takayanagi (North-Holland, Amsterdam, 1980), p. 453.
[32]T. G. Heil, S. E. Butler, and A. Dalgarno, Phys. Rev. A 23, 1100 (1981).